OBSERVABLES IN UNPOLARIZED AND POLARIZED VIRTUAL COMPTON SCATTERING

A. METZ

Institut für Theoretische Physik, Ruprecht Karls-Universität Philosophenweg 19, D-69120 Heidelberg, Germany E-mail: metz@frodo.tphys.uni-heidelberg.de

B. PASQUINI

Institut für Kernphysik, Johannes Gutenberg-Universität J. J. Becher-Weg 45, D-55099 Mainz, Germany E-mail: pasquini@kph.uni-mainz.de

D. DRECHSEL

Institut für Kernphysik, Johannes Gutenberg-Universität J. J. Becher-Weg 45, D-55099 Mainz, Germany E-mail: drechsel@kph.uni-mainz.de

Below pion threshold virtual Compton scattering off the nucleon gives access to the generalized electromagnetic polarizabilities. Different theoretical results for the generalized polarizabilities have been compared. In particular, the influence of the generalized polarizabilities on the unpolarized cross section and on double polarization observables has been investigated. Predictions for these observables have been obtained in the linear sigma model and chiral perturbation theory.

1 Introduction

Compton scattering has a long history as an interesting tool to investigate the nucleon's structure. Though it has been applied in different kinematical regions, Compton scattering is of particular interest below the threshold of pion production, where the electromagnetic polarizabilities of the nucleon can be studied. While in the past the main focus was on real Compton scattering (RCS), recently much effort has been devoted to virtual Compton scattering (VCS), $\gamma^* + N \to \gamma + N$, with a virtual photon γ^* in the initial state and a real photon γ in the final state. In comparison to RCS, the VCS reaction contains much more information because of the variable mass and the additional longitudinal polarization of the virtual photon.

As shown in Fig. 1, VCS can be realized experimentally by electron-nucleon bremsstrahlung, $e+N \rightarrow e'+N'+\gamma$. Besides the VCS mechanism, the bremsstrahlung contains the Bethe-Heitler scattering (BH), where the real photon is emitted from the incoming or outgoing electron. Therefore, the total amplitude $T^{ee'\gamma}$ is the coherent sum of the VCS amplitude T^{VCS} and the BH

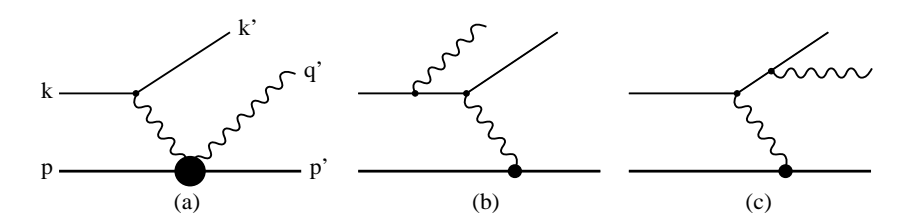


Figure 1: Feynman diagrams of the reaction $e(k) + N(p) \rightarrow e'(k') + N'(p') + \gamma(q')$. (a): the VCS contribution containing the Born and residual amplitudes. (b) and (c): Bethe-Heitler scattering.

amplitude
$$T^{BH}$$
,
$$T^{ee'\gamma} = T^{VCS} + T^{BH} \,. \tag{1}$$

If not stated differently, we use the cm frame of the final state photon and nucleon throughout this article. The 4-momenta of the incoming photon and nucleon are denoted by $q^{\mu}=(\omega,\vec{q})$ and $p^{\mu}=(E,-\vec{q})$, respectively, while the outgoing particles are characterized by $q'^{\mu}=(\omega',\vec{q}')$ and $p'^{\mu}=(E',-\vec{q}')$. We also define $Q^2\equiv -q^2$ and $\bar{q}\equiv |\vec{q}|$. For the following discussion it is convenient to introduce the quantity

$$Q_0^2 \equiv Q^2|_{\omega'=0} = 2m_N \left[\sqrt{\bar{q}^2 + m_N^2} - m_N \right]. \tag{2}$$

According to Eq. (2), the variable Q_0^2 can be replaced by \bar{q} and vice versa.

Below pion threshold, the analysis of both RCS and VCS is based on low energy theorems, which rely on fundamental symmetries as Lorentz invariance, gauge invariance and crossing symmetry. The decomposition of the scattering amplitude into a Born contribution and the residual part plays an important role in the derivation of these theorems. In the case of VCS we have

$$T^{VCS} = T_B^{VCS} + T_R^{VCS}, (3)$$

where the Born amplitude T_B^{VCS} shows the typical $1/\omega'$ singularity of bremsstrahlung, while the residual amplitude T_R^{VCS} is proportional to ω' in the low energy limit ^{1,2}. The Born amplitude is entirely determined by the nucleon mass, its charge and the electromagnetic form factors, G_E and G_M , i.e., by definition T_B^{VCS} contains only properties of the nucleon in its ground state. The influence of the excitation spectrum enters through the residual amplitude which can be parametrized by the generalized polarizabilities (GPs) of the nucleon ¹. To leading order in ω' , there appear 10 GPs in T_R^{VCS} . These GPs depend on Q_0^2 or \bar{q} and are related with the electromagnetic polarizabilities of RCS whose leading contribution is completely determined by the well

known electric (α) and magnetic (β) polarizabilities. We discuss the GPs in the following section in more details.

The measurement of the GPs requires data with a very high accuracy which can only be obtained by means of the new electron accelerator facilities like MAMI, MIT-Bates and Jefferson Lab. The VCS reaction has already been measured at MAMI³ for $\bar{q}=600$ MeV, it will be investigated at $\bar{q}=240$ MeV at MIT-Bates⁴, while the activities at Jefferson Lab⁵ will concentrate on the region of $\bar{q}\approx 1$ GeV. Very recently, the first preliminary results for $\alpha(\bar{q})$ and $\beta(\bar{q})$ have been extracted from the MAMI experiment⁶.

On the theoretical side the GPs were predicted by various approaches. Calculations of all GPs have been performed in the nonrelativistic constituent quark model (CQM) 1,7 , chiral perturbation theory in the heavy baryon formalism (HBChPT) including the Δ resonance as a dynamical degree of freedom 8,9,10 , and in the one-loop approximation of the linear sigma model (LSM) 11,12 . The \bar{q} behaviour of α and β was determined in an effective Lagrangian model 13 containing several resonances and the exchange of π^0 and σ mesons in the t channel. In addition, there exists a Skyrme model prediction of $\alpha(\bar{q})^{14}$, while the paramagnetic part of $\beta(\bar{q})$ was calculated in a relativistic quark-model formulated in the light-front dynamics 15 .

The influence of the GPs on observables as the unpolarized cross section of the reaction $p(e,e'p')\gamma$ and asymmetries for beam-recoil polarization, $p(\vec{e},e'\vec{p}')\gamma$, has been studied in the effective Lagrangian approach by Vanderhaeghen ^{13,16}. In these studies the contributions to the amplitude T_R^{VCS} were investigated to all orders in ω' , i.e., the effects of higher order GPs were automatically incorporated. In contrast to this, we will only consider the dipole approximation to T_R^{VCS} . Regarding the validity of this approximation, see the discussion in sec. 2.1. In the unpolarized case, the ω' dependence of the effect due to the GPs was previously calculated in HBChPT ¹⁰. In addition to unpolarized cross sections, we also predict asymmetries of beam-target polarization, $\vec{p}(\vec{e},e'p')\gamma$, which can be explored at Bates using the BLAST target-detector system. We will show predictions of the LSM and HBChPT focusing on the influence of the GPs as function of the $\gamma^*\gamma$ scattering angle.

2 Generalized Polarizabilities

2.1 Definitions and Constraints

The concept of GPs was first introduced in connection with nuclear targets ¹⁷ and has recently been discussed in detail for the specific case of the nucleon ¹. The GPs can be defined through the multipoles $H_R^{(\rho'L',\rho L)S}(\omega',\bar{q})$ of the residual amplitude. In the notation of the multipoles, $\rho(\rho')$ denotes the type of the

Table 1: Possible transitions to VCS in the case of the dipole approximation for the real photon (E: electric, M: magnetic, C: Coulomb). The last column gives the notation of the GPs.

final photon	initial photon	S	GPs
E1	C1	0,1	$P^{(01,01)S}$
E1	E1	0,1	$P^{(01,01)S}, \hat{P}^{(01,1)S}$
E1	M2	1	$P^{(01,12)1}$
M1	M1	0,1	$P^{(11,11)S}$
M1	C0	1	$P^{(11,00)1}$
M1	C2	1	$P^{(11,02)1}$
M1	E2	1	$P^{(11,02)1}, \hat{P}^{(11,2)1}$

incoming (outgoing) photon ($\rho=0$: Coulomb, $\rho=1$: magnetic, $\rho=2$: electric) while $L\left(L'\right)$ refers to the angular momentum of the initial (final) photon. The quantum number S indicates a no spin–flip (S=0) or a spin–flip (S=1) transition.

In order to define the GPs it is suitable to replace all electric transitions. As a consequence one introduces the socalled mixed multipoles $\hat{H}_R^{(\rho'L',L)S}$ describing a well defined mixture of an electric and a charge transition in the initial state. More details on this technique can be found in the literature ^{1,18}. The GPs are finally given by

$$P^{(\rho'L',\rho L)S}(\bar{q}) = \left[\frac{1}{\omega'^{L'}\bar{q}^{L}}H_{R}^{(\rho'L',\rho L)S}(\omega',\bar{q})\right]_{\omega'=0} (\rho,\rho'=0,1),$$

$$\hat{P}^{(\rho'L',L)S}(\bar{q}) = \left[\frac{1}{\omega'^{L'}\bar{q}^{L+1}}\hat{H}_{R}^{(\rho'L',L)S}(\omega',\bar{q})\right]_{\omega'=0} (\rho'=0,1), \qquad (4)$$

and carry the same quantum numbers as the corresponding multipoles ¹. In the dipole approximation for the real photon (L'=1), selection rules due to parity and angular momentum conservation lead to the ten possible transitions listed in Table 2.1, 3 scalar GPs (S=0) and 7 vector GPs (S=1). Note that the dipole approximation is equivalent to keeping only the leading (linear) order in ω' for the residual amplitude. Since the relevant expansion parameter is ω'/m_{π} , the dipole approximation describes the experimental data for RCS only if $\omega' \leq 60$ MeV, well below the pion mass m_{π} . However, in VCS the situation is more complicated. As has been pointed out recently, higher order terms in ω' become more important if \bar{q} is of the same order of magnitude as ω'^{19} . Therefore, beyond the restriction given by the pion mass, the condition

 $\bar{q}\gg\omega'$ should be fulfilled to guarantee the validity of the dipole approximation in VCS.

In part the GPs are related to the electromagnetic polarizabilities which govern the low-energy expansion of the RCS amplitude. The scalar polarizabilities $P^{(01,01)0}(\bar{q})$ and $P^{(11,11)0}(\bar{q})$ generalize α and β to the case of virtual photons,

$$P^{(01,01)0}(\bar{q}) = -\frac{4\pi}{e^2} \frac{\sqrt{2}}{\sqrt{3}} \alpha(\bar{q}) , \quad P^{(11,11)0}(\bar{q}) = -\frac{4\pi}{e^2} \frac{\sqrt{8}}{\sqrt{3}} \beta(\bar{q}) , \qquad (5)$$

with $e^2/4\pi \approx 1/137$. Two of the vector GPs are connected with the four spin polarizabilities γ_i of RCS as defined by Ragusa ²⁰. The relations read ²¹

$$P^{(01,12)1}(0) = -\frac{4\pi}{e^2} \frac{\sqrt{2}}{3} \gamma_3, \quad P^{(11,02)1}(0) = -\frac{4\pi}{e^2} \frac{2\sqrt{2}}{3\sqrt{3}} (\gamma_2 + \gamma_4). \tag{6}$$

The remaining two combinations of spin polarizabilities of RCS can not be related to the GPs in the dipole approximation. In particular, the forward spin-polarizability $\gamma = \gamma_1 - \gamma_2 - 2\gamma_4$ is not contained in this kinematical limit of VCS²¹.

As has been shown by our explicit calculation in the LSM 11 and later by a model-independent analysis 22 based on charge conjugation symmetry and nucleon crossing, the ten GPs have to satisfy four constraints. For instance, the three scalar GPs obey the condition

$$\frac{e^2}{4\pi}\hat{P}^{(01,1)0}(\bar{q}) = -\frac{Q_0^2}{3m_N\bar{q}^2} \left[\alpha(\bar{q}) + \beta(\bar{q})\right]. \tag{7}$$

Similarly, there are three relations among the vector GPs ^{12,21}. In addition to these relations, the vector GPs fulfill specific constraints at $\bar{q} = 0$. Three vector GPs vanish at the origin,

$$P^{(01,01)1}(0) = P^{(11,11)1}(0) = P^{(11,00)1}(0) = 0, (8)$$

while the remaining four satisfy the condition

$$P^{(01,12)1}(0) + \sqrt{3}P^{(11,02)1}(0) - \sqrt{3}\hat{P}^{(01,1)1}(0) - 2\sqrt{5}m_N\hat{P}^{(11,2)1}(0) = 0. \quad (9)$$

Because of the constraints, only six instead of ten GPs are independent. Though there is some arbitrariness in the selection of the independent GPs, a natural choice has been proposed in a recent review article of Guichon and Vanderhaeghen 18 . The authors eliminate the three mixed GPs $\hat{P}^{(01,1)0}$, $\hat{P}^{(01,1)1}$, $\hat{P}^{(11,2)1}$ and the quantity $P^{(11,00)1}$. In the following discussion we focus on the remaining six GPs.

2.2 Results and Discussion

Both nonresonant and resonant excitations of the nucleon contribute to the GPs. However, in the kinematical region of Compton scattering below pion threshold, the nonresonant s-wave production of pions is of particular importance. This process is determined by chiral symmetry and can be described by pion-loop diagrams in ChPT or in the LSM. On the other side, we also expect large influences of resonances. In particular, the $\Delta(1232)$ and the $D_{13}(1520)$ resonances, which are both clearly visible in the photoabsorption spectrum of the nucleon, significantly contribute to some of the GPs 1,15 .

In addition to these excitations of the nucleon, the chiral anomaly (π_0 exchange in the t channel) is quite essential in the case of the vector GPs. At low values of \bar{q} , the shape for three of the four independent vector GPs is strongly governed by the anomaly ^{9,12}, as will be discussed in sect. 3.

Before comparing the numerical predictions of different approaches, we discuss the analytical results for the GPs obtained in the LSM 11,12 and in HBChPT to lowest order $(\mathcal{O}(p^3))^{8,10}$. The chiral expansions of the GPs at $Q_0^2=0$ contain the most instructive information. As an example, we find for the electric and magnetic polarizabilities of the proton in the case of the one-loop approximation to the LSM

$$\alpha_p(0) = \frac{e^2 g_{\pi N}^2}{192\pi^3 m_N^3} \left[\frac{5\pi}{2\mu} + 18 \ln \mu + \frac{33}{2} + \mathcal{O}(\mu) \right]$$

$$= \left[13.6 - 8.8 + 4.2 + \mathcal{O}(\mu) \right] \times 10^{-4} \,\text{fm}^3,$$

$$\beta_p(0) = \frac{e^2 g_{\pi N}^2}{192\pi^3 m_N^3} \left[\frac{\pi}{4\mu} + 18 \ln \mu + \frac{63}{2} + \mathcal{O}(\mu) \right]$$

$$= \left[1.4 - 8.8 + 8.1 + \mathcal{O}(\mu) \right] \times 10^{-4} \,\text{fm}^3, \tag{10}$$

with $\mu = m_{\pi}/m_N$ and $g_{\pi N} = m_N g_A/F_{\pi} \approx 13.4$ the pseudoscalar pion–nucleon coupling constant. It is interesting to note that the chiral expansions of Eq. (10) agree with a one-loop calculation of relativistic ChPT²³ to all orders in μ . The corresponding results of HBChPT to $\mathcal{O}(p^3)$ are given by the leading term in Eq. (10). Similar chiral expansions have been obtained for all of the GPs and for their derivatives with respect to Q_0^2 ^{10,11,12}. Both chiral approaches completely agree in the sense that in all cases the leading contribution of the expansion in the LSM is exactly the result of HBChPT to $\mathcal{O}(p^3)$.

The chiral expansions of the polarizabilities show a common feature: compared to the leading term the contribution next to leading order has a different sign. Such an alternating behaviour of the chiral series can also be observed in

HBChPT to $\mathcal{O}(p^4)$ for $\alpha(0)$ and $\beta(0)$ if one neglects counterterm contributions which arise from resonance saturation 24 .

The pion cloud of the nucleon causes a diamagnetic response and therefore a negative magnetic polarizability. According to Eq. (10), this diamagnetic part of β is not contained in the leading chiral contribution but in the terms next to leading order (logarithmic plus constant term). In Fig. 2 we plot the GPs as a function of Q_0^2 calculated in the CQM⁷, in HBChPT to order $\mathcal{O}(p^3)^{9,10}$ and in the LSM ^{11,12}. We first consider the scalar polarizabilities α and β . At the real photon point ($Q_0^2 = 0$), the LSM underestimates the empirical values ²⁵ ($\alpha_p^{exp}(0) = 12.1 \pm 1.0 \times 10^{-4} \, \text{fm}^3$, $\beta_p^{exp}(0) = 2.1 \mp 1.0 \times 10^{-4} \, \text{fm}^3$) to some degree. This drawback can be attributed to the neglect of t-channel exchange of heavier or more meson states, and of nucleon resonances in the s-channel, e.g. $D_{13}(1520)$ in the case of α and $\Delta(1232)$ with its strong paramagnetic (quark spin-flip) contribution to β .

In HBChPT the results at the real photon point are in good agreement with the experiment. However, at least for the magnetic polarizability, this agreement is somewhat accidental because both the paramagnetic contribution of the $\Delta(1232)$ and the main diamagnetic contribution of the pion cloud have not been taken into account. The results for α and β to $\mathcal{O}(p^4)$ show a large cancellation between diamagnetic and paramagnetic terms ²⁴, where the final results for the proton are $\alpha_p = 10.5 \pm 2.0 \times 10^{-4} \, \mathrm{fm}^3$ and $\beta_p = 3.5 \pm 3.6 \times 10^{-4} \, \mathrm{fm}^3$. In a recent development the Δ was incorporated in to the effective chiral lagrangian. Unfortunately, this formalism predicts too large numbers for α and β in a calculation to $\mathcal{O}(\epsilon^3)$ ^{9,10}.

Though the values of α and β at the real photon point are different for HBChPT and the LSM, both chiral calculations predict a very similar Q_0^2 behaviour for these polarizabilities. In the CQM the Q_0^2 dependence is rather different in comparison to the chiral calculations, the discrepancy being strongest in the case of β .

At low Q_0^2 , the polarizability $P_p^{(11,11)1}$ is very large in the CQM in contrast to the chiral calculations. This behaviour is due to the neglect of diamagnetic contributions in the CQM. Furthermore, the CQM predicts finite values for the GPs $P_p^{(11,11)1}$ and $P_p^{(01,01)1}$ at the origin and therefore violates the model-independent constraints of Eq. (8). The most remarkable discrepancy between the CQM and the chiral predictions is in the absolute values of $P_p^{(01,01)1}$ and $P_p^{(11,02)1}$ which differ by two orders of magnitude.

3 Observables

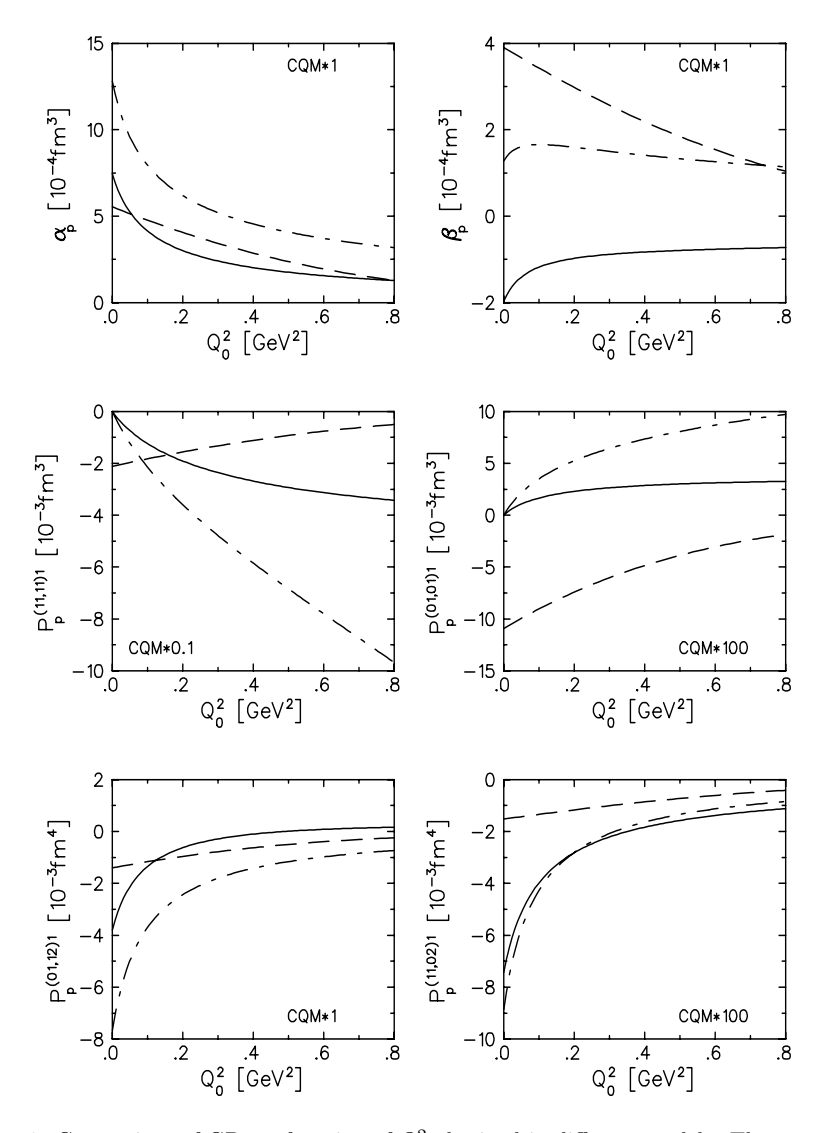


Figure 2: Comparison of GPs as function of Q_0^2 obtained in different models. The anomaly is not included. Solid line: LSM, dashed line: CQM, dash–dotted line: HBChPT to $\mathcal{O}(p^3)$. Note that the CQM results have been scaled.

3.1 Formalism

In the case of the unpolarized reaction $p(e, e'p')\gamma$ we consider the five-fold differential cross section,

$$\frac{d^{5}\sigma}{d|\vec{k}'_{lab}|(d\Omega_{k'})_{lab}(d\Omega_{p'})_{cm}} = K_{1} \frac{1}{4} \sum_{spins} |T^{ee'\gamma}|^{2},$$
(11)

where K_1 represents a phase space factor. The cross section depends on the five variables

$$\omega', \quad \bar{q}, \quad \theta, \quad \phi, \quad \epsilon,$$
 (12)

with θ the angle between the two photons, ϕ the azimuthal angle between the leptonic plane and the reaction plane, and ϵ the transverse polarization of the virtual photon. According to Eqs. (1) and (3), the scattering amplitude $T^{ee'\gamma}$ consists of three parts,

$$T^{ee'\gamma} = T^{BH} + T_R^{VCS} + T_R^{VCS}. \tag{13}$$

As explained in sect. 1, the "background" amplitudes T^{BH} and T^{VCS}_B behave like $1/\omega'$ in the low energy limit, while T^{VCS}_R is proportional to ω' . Therefore, the expansion of the spin-averaged matrix element reads

$$\frac{1}{4} \sum_{snins} |T^{ee'\gamma}|^2 = \frac{C_{-2}^{BH+Born}}{\omega'^2} + \frac{C_{-1}^{BH+Born}}{\omega'} + C_0^{BH+Born} + C_0^{Pol} + \mathcal{O}(\omega'), \quad (14)$$

where the coefficients $C_{-2}^{BH+Born}$, $C_{-1}^{BH+Born}$ and $C_{0}^{BH+Born}$ are entirely determined by the background. The coefficient C_{0}^{Pol} results from the interference of the singular part of the background term with the leading term of T_{R}^{VCS} and contains the information on the GPs. It can be expressed in terms of four structure functions 1 ,

$$C_0^{Pol} = K_2(\epsilon, \bar{q}) \Big[v_1 \Big(\epsilon P_{LL}(\bar{q}) - P_{TT}(\bar{q}) \Big) + v_2 \sqrt{2\epsilon (1+\epsilon)} P_{LT}(\bar{q}) + v_3 \sqrt{2\epsilon (1+\epsilon)} P'_{LT}(\bar{q}) \Big],$$

$$(15)$$

with kinematical factors v_i depending on \bar{q} , θ , ϕ and ϵ . The structure functions contain the GPs in combination with the elastic form factors of the nucleon. Using the results of Ref. ²¹, the structure functions P_{LT} and P'_{LT} are mutually dependent via the relation

$$P_{LT}(\bar{q}) = \frac{2m_N \bar{q}}{Q_0^2} P'_{LT}(\bar{q}).$$
 (16)

As a consequence, the coefficient C_0^{Pol} contains only three independent structure functions, thus leading to information on three of the six independent GPs.

In order to disentangle the remaining polarizabilities one has to resort to double polarization observables. As has been suggested by Vanderhaeghen 16 , the reaction $p(\vec{e},e'\vec{p}')\gamma$ can be used to extract the remaining three polarizabilities. Instead of measuring recoil polarization, the same information can be gained by the reaction $\vec{p}(\vec{e},e'p')\gamma$. We focus the attention on the observables for beam-target polarization in order to give some guidance for a possible experiment with the BLAST facility at MIT-Bates. To this end we consider the target (double) asymmetries

$$T^{(i)} = \frac{\left[\sigma_{h=\frac{1}{2},m_i=\frac{1}{2}} - \sigma_{h=\frac{1}{2},m_i=-\frac{1}{2}}\right] - \left[\sigma_{h=-\frac{1}{2},m_i=\frac{1}{2}} - \sigma_{h=-\frac{1}{2},m_i=-\frac{1}{2}}\right]}{\left[\sigma_{h=\frac{1}{2},m_i=\frac{1}{2}} + \sigma_{h=\frac{1}{2},m_i=-\frac{1}{2}}\right] + \left[\sigma_{h=-\frac{1}{2},m_i=\frac{1}{2}} + \sigma_{h=-\frac{1}{2},m_i=-\frac{1}{2}}\right]}, \quad (17)$$

where h is the electron helicity and m_i (i = x, y, z) is the spin-projection of the nucleon target with respect to the coordinate system

$$\hat{e}_x = \frac{\hat{q}' - \cos\vartheta\,\hat{q}}{\sin\vartheta}, \quad \hat{e}_y = \frac{\hat{q}\times\hat{q}'}{\sin\vartheta}, \quad \hat{e}_z = \hat{q}.$$
 (18)

As in the unpolarized case, one can perform a low energy expansion for the numerator of the asymmetries leading to expansion coefficients $C_{0(i,0)}^{Pol}$. In terms of structure functions these coefficients read

$$C_{0(z,0)}^{Pol} = 4K_{2}(\epsilon, \bar{q}) \left[v_{1} \sqrt{1 - \epsilon^{2}} P_{TT}^{(z,0)}(\bar{q}) + v_{2} \sqrt{2\epsilon(1 - \epsilon)} P_{LT}^{(z,0)}(\bar{q}) + v_{3} \sqrt{2\epsilon(1 - \epsilon)} P_{LT}^{(z,0)}(\bar{q}) \right],$$

$$(19)$$

$$C_{0(x,0)}^{Pol} = 4K_{2}(\epsilon, \bar{q}) \left[v_{1}^{x} \sqrt{2\epsilon(1 - \epsilon)} P_{LT}^{(\perp,0)}(\bar{q}) + v_{2}^{x} \sqrt{1 - \epsilon^{2}} P_{TT}^{(\perp,0)}(\bar{q}) + v_{3}^{x} \sqrt{1 - \epsilon^{2}} P_{TT}^{(\perp,0)}(\bar{q}) + v_{4}^{x} \sqrt{2\epsilon(1 - \epsilon)} P_{LT}^{(\perp,0)} \right].$$

$$(20)$$

A similar decomposition of $C^{Pol}_{0(y,0)}$ contains the same structure functions as $C^{Pol}_{0(x,0)}$ in Eq. (19), however with new kinematical factors v^y_i . Note that the kinematical factors for target polarization in z-direction are the same as in the unpolarized case. Altogether one obtains three new independent structure functions, $P^{(z,0)}_{LT}$, $P^{(z,0)}_{LT}$ and $P^{(\perp,0)}_{LT}$. The extraction of $P^{(\perp,0)}_{LT}$ requires an out-of-plane measurement since $v^x_4 \to 0$ for $\phi \to 0^\circ$. This situation is quite analogous to the case of double polarization asymmetries with recoil polarization 16 , whose expansion coefficients contain the same kinematical factors as for target polarization, while the corresponding structure functions may have

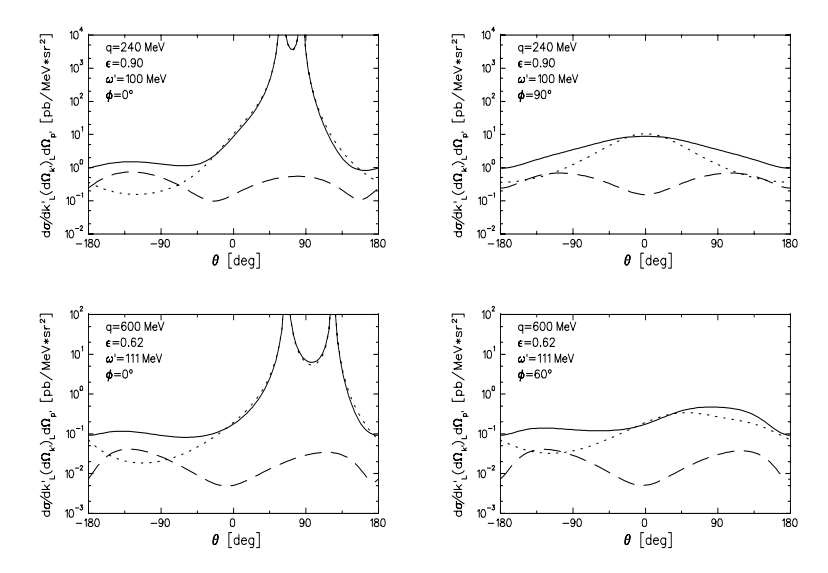


Figure 3: Background cross section for the Bates kinematics and the MAMI kinematics as function of the scattering angle θ . Dashed line: VCS Born contribution, dotted line: Bethe-Heitler contribution, full line: complete background cross section.

a somewhat different appearance. The explicit expressions for the coefficients $C_{0(i,0)}^{Pol}$ will be presented in an upcoming publication ²⁶.

3.2 Results and Discussion

In the following numerical studies we concentrate on two different kinematics: (I) the Bates kinematics with $\bar{q}=240\,\mathrm{MeV}$, $\epsilon=0.9$ and $\omega'=100\,\mathrm{MeV}$ and (II) the MAMI kinematics with $\bar{q}=600\,\mathrm{MeV}$, $\epsilon=0.62$ and $\omega'=111\,\mathrm{MeV}$. Both sets of variables have been explored in the unpolarized experiments at Bates and MAMI. The main difference between the two kinematics is in the values of \bar{q} and ϵ , while the difference in ω' will be neglected in the discussion below. In our analysis, the observables are always calculated as function of the scattering angle θ . In addition, we distinguish between in-plane ($\phi=0$) and the 90° degree out-of-plane kinematics for the Bates kinematics, while in the case of the MAMI kinematics the in-plane and 60° degree out-of-plane cases have been investigated. Results for the background cross section are shown in Fig. 3, with the separate contributions from the BH and the VCS Born amplitude. For the elastic form factors of the proton we used the parametrization of Ref. 27. In the case of in-plane kinematics, the angular dependence of the BH cross sec-

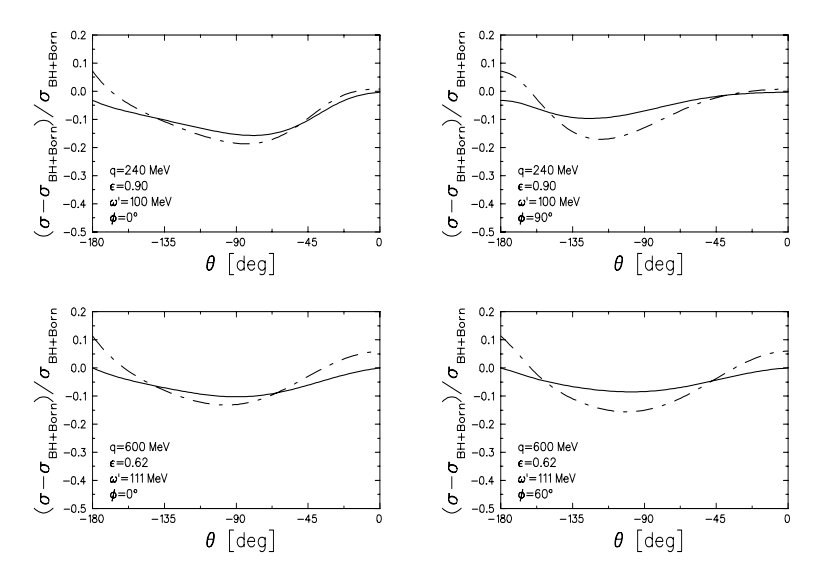


Figure 4: Influence of the GPs on the unpolarized cross section of the reaction $p(e,e'p')\gamma$ for Bates and MAMI kinematics. Full line: LSM result, dash-dotted line: HBChPT result. The quantity $\sigma - \sigma_{BH+Born}$ represents the contribution of the coefficient C_0^{Pol} of Eq. (15) to the cross section.

tion is characterized by two peaks occurring for the real photons emitted along the direction of the initial or final electrons. In these regions, the BH term gives the overwhelming contribution to the background cross section, while it becomes much smaller at negative values of θ . For out-of-plane configurations the two peaks disappear, and in the case of the Bates kinematics the angular distribution of the background term is almost symmetrical around $\theta=0$. In order to increase the sensitivity to the GPs, the region of negative scattering angles corresponding to photon emission in the half-plane opposite to the outgoing electron has to be explored. In comparison to the MAMI kinematics, the background cross section is one order of magnitude higher in the Bates case, whereas the θ dependence of the background is similar for both kinematics.

For the LSM and HBChPT the relative influence of the GPs on the unpolarized cross section has been plotted in Fig. 4. As is to be expected, HBChPT generally predicts larger effects than the LSM. In both calculations the influence of the GPs is negative for a large region of θ , leading to a reduction of the total cross section. For the unpolarized case the anomaly gives no contribution as long as only the leading order in ω' is taken into account.

For the Bates kinematics the GPs change the cross section by about 20%, the

effect being almost completely given by $\alpha(\bar{q})$. The influence of the GPs for the MAMI kinematics is of the order of 15%. In this case the LSM predicts that only 60% of the signal are due to the electric polarizability. Since one aims at cross section measurements with a relative error of about 2%, the calculated effects should be detected. However, there are two problems which render the measurement of the GPs more difficult: (I) the effect of the GPs strongly increases with ω' . At $\omega' = 70\,\mathrm{MeV}$, e.g., the effects shown in Fig. 4 reduce by roughly 50%. For higher values of ω' , where the signal is larger, higher order terms of the residual amplitude can no longer be neglected (see also the corresponding discussion in sect. 2.1). In this case the challenging task is the reliable extraction of the leading order contribution in which one is interested. (II) Independent of the value of ω' there are large radiative corrections 28 . These corrections result in a 20% contribution to the cross section which is of the same order of magnitude as the influence of the GPs, thus complicating the separation of background and GP effects.

In Fig. 5 we show the GP contribution to the target asymmetries $T^{(z)}$ and $T^{(x)}$ for both LSM and HBChPT, without taking account of the anomaly contribution. Obviously, larger effects can be expected in the case of $T^{(x)}$. While in the unpolarized cross section the GP effect was larger for Bates kinematics, we now observe the opposite situation for the asymmetries. Here the maximum signature is about 10% for the MAMI kinematics but only about 3% for the Bates kinematics. The different behaviour between the unpolarized and the polarized case has the following explanation: In Fig. 4 we have seen that the background, which determines the denominator of the asymmetries, is one order of magnitude larger for the Bates kinematics. On the other side, the influence of the GPs in the numerator of the asymmetries increases much less when going from Bates to MAMI kinematics, while the influence of the GPs on the unpolarized cross section also strongly increases by changing the kinematics, in particular due to the strong \bar{q} dependence of the electric polarizability. More details of this discussion will be presented in Ref. 26 .

In Fig. 6 we display the anomaly contribution to the asymmetries as predicted by the LSM. Since the influence of the anomaly is strongly decreasing with increasing \bar{q} , the largest effect shows up for the Bates kinematics. In this case the shape of the asymmetry $T^{(z)}$ is completely changed by the anomaly. Though for the MAMI kinematics the anomaly is less dominant, its influence is still quite sizeable.

We conclude that a full determination of the GPs will require double polarization experiments, polarized electrons and target or recoil polarization, in addition to the unpolarized experiments. Given the projected accuracy of the experiments, one should be able to measure the GPs in spite of a large

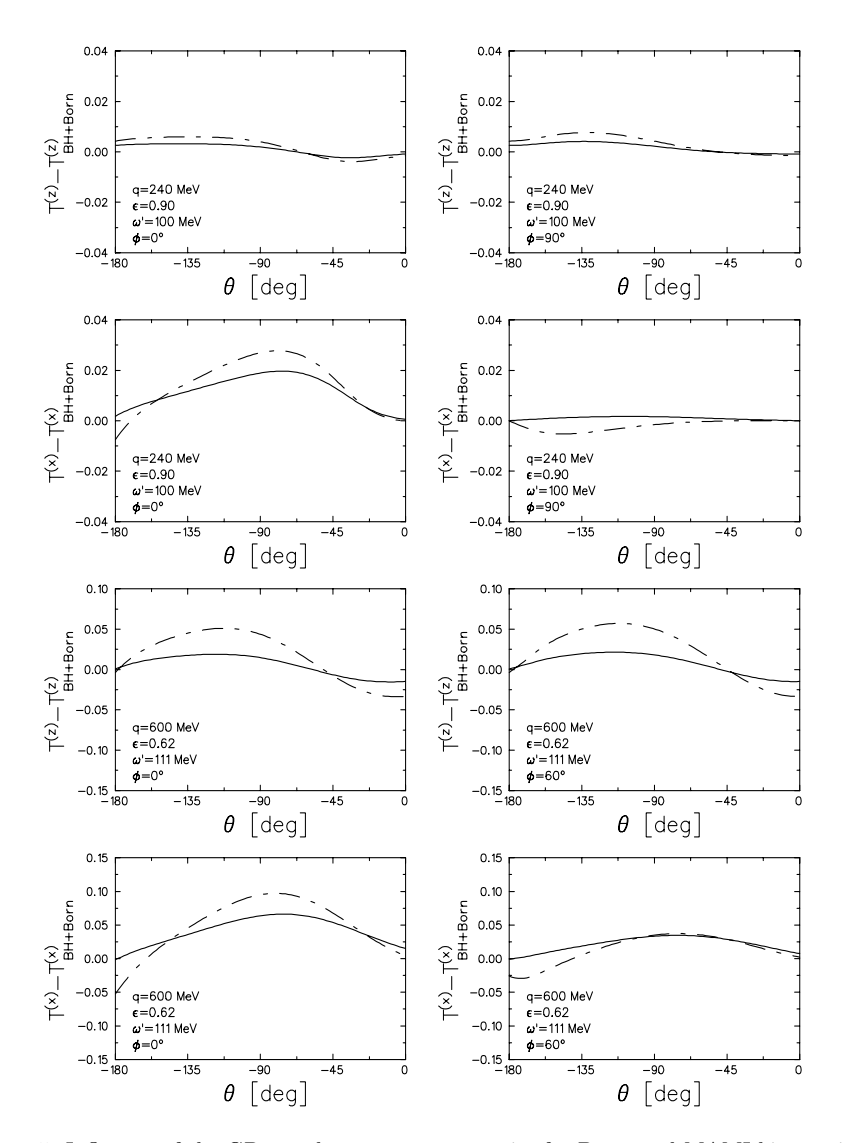


Figure 5: Influence of the GPs on the target asymmetries for Bates and MAMI kinematics. Full line: LSM result, dash-dotted line: HBChPT result. The quantities $T^{(z)} - T^{(z)}_{BH+Born}$ and $T^{(x)} - T^{(x)}_{BH+Born}$ represent the contribution of the coefficients $C^{Pol}_{0(z,0)}$ and $C^{Pol}_{0(x,0)}$ in Eqs. (19) and (20), respectively.

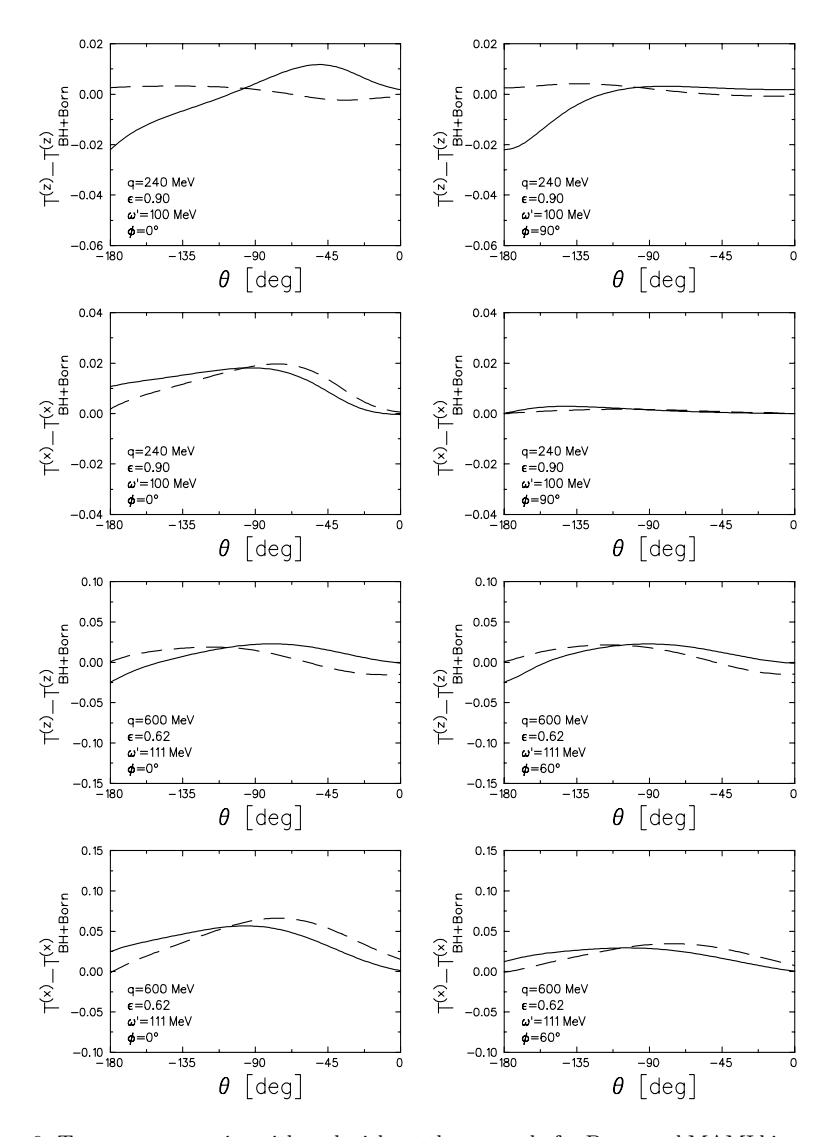


Figure 6: Target asymmetries with and without the anomaly for Bates and MAMI kinematics as obtained in the LSM. Full line: anomaly included, dashed line: without anomaly.

background. Since the momentum dependence of the GPs is predicted quite differently by various models, such precision experiments will be invaluable to restrict the model parameters, and, quite generally, as further benchmarks of the nucleon's structure.

Acknowledgments

The authors thank M. Vanderhaeghen for useful discussions concerning the formalism of the observables.

References

- P.A.M. Guichon, G.Q. Liu and A.W. Thomas, Nucl. Phys. A 591, 606 (1995).
- 2. S. Scherer, A.Yu. Korchin and J.H. Koch, *Phys. Rev.* C **54**, 904 (1996).
- 3. G. Audit et al., MAMI proposal on Nucleon structure study by Virtual Compton Scattering (1995).
- 4. B. Asavapibhop et al., MIT-Bates proposal on *Virtual Compton Scattering on the Proton below Pion Threshold* (1997).
- 5. G. Audit et. al., CEBAF proposal PR-93-050 (1993).
- 6. T. Walcher, contribution to this conference.
- G.Q. Liu, A.W. Thomas and P.A.M. Guichon, Austr. J. Phys. 49, 905, (1996).
- T.R. Hemmert, B.R. Holstein, G. Knöchlein and S. Scherer, *Phys. Rev.* D 55, 2630 (1997).
- 9. T.R. Hemmert, B.R. Holstein, G. Knöchlein and S. Scherer, *Phys. Rev. Lett.* **79**, 22 (1997).
- 10. G. Knöchlein, PhD thesis on Virtual Compton Scattering off the Nucleon and Chiral Perturbation Theory, Shaker Verlag, Aachen (1997).
- 11. A. Metz and D. Drechsel, Z. Phys. A **356**, 351 (1996).
- 12. A. Metz and D. Drechsel, Z. Phys. A **359**, 165 (1997).
- 13. M. Vanderhaeghen, *Phys. Lett. B* **368**, 13 (1996).
- 14. M. Kim and D.-P. Min, hep-ph/9704381.
- 15. B. Pasquini and G. Salmé, *Phys. Rev.* C **57**, 2589 (1998).
- 16. M. Vanderhaeghen, *Phys. Lett. B* **402**, 243 (1997).
- 17. H. Arenhövel and D. Drechsel, Nucl. Phys. A 233, 153 (1974).
- 18. P.A.M. Guichon and M. Vanderhaeghen, Prog. Part. Nucl. Phys. 41 (1998).
- 19. D. Drechsel, G. Knöchlein, A.Yu. Korchin, A. Metz and S. Scherer, nucl-th/9804078, to appear in Phys. Rev. C 58 (1998).
- 20. S. Ragusa, Phys. Rev. D 47, 3757 (1993); Phys. Rev. D 49, 3157 (1994).

- 21. D. Drechsel, G. Knöchlein, A.Yu. Korchin, A. Metz and S. Scherer, *Phys. Rev.* C **57**, 941 (1998).
- 22. D. Drechsel, G. Knöchlein, A. Metz and S. Scherer, *Phys. Rev.* C $\bf 55$, 424 (1997).
- 23. V. Bernard, N. Kaiser and U.G. Meißner, Nucl. Phys. B 373, 346 (1992).
- 24. V. Bernard, N. Kaiser, U.G. Meißner and A. Schmidt, *Phys. Lett.* B **319**, 269 (1993); *Z. Phys.* A **348**, 317 (1994).
- 25. B.E. MacGibbon et al., Phys. Rev. C 52, 2097 (1995).
- 26. D. Drechsel, A. Metz and B. Pasquini, in preparation.
- 27. P. Mergell, U.G. Meißner and D. Drechsel, *Nucl. Phys.* A **596**, 367 (1996).
- 28. M. Vanderhaeghen, D. Lhuillier, D. Marchand and J. Van de Wiele, in preparation.